

*Short Communication*

## **An Investigation of Nanostructure Morphology in the Zinc-Air Cell Method as a Function of Electrolyte Concentration**

T.D Malevu\*, R.O Ocaya

Department of Physics, University of the Free State (QwaQwa Campus), P. Bag X13, Phuthaditjhaba 9866.

\*E-mail: [MalevuTD@qwa.ufs.ac.za](mailto:MalevuTD@qwa.ufs.ac.za)

*Received:* 6 February 2015 / *Accepted:* 28 February 2015 / *Published:* 23 March 2015

---

Earlier studies of the formation of ZnO nanostructures using the zinc-air cell method have indicated a rich presence of nanostructures such as hierarchical nanowires, nanorods, flower-like and nano-needles with an inherent hexagonal wurtzite structure. Controlling the growth orientation of semiconductor nanostructure arrays, particularly nanowires bears vital importance for their applicability in the fields nano-electronics. The ZAC system method appears to be almost free from impurities, although post-heating and annealing may contribute some impurities, the most notable being carbon. Other effects, such as UV-Visible wavelength absorption have been observed as the likely result of structural defects and intrinsic excitons. This article therefore attempts to correlate the observed structural forms to the main determinants in the ZAC method thereby providing a reference point for the further synthesis of these forms using the method.

---

**Keywords:** ZnO, nanostructures, zinc-air cell system, annealing

### **1. INTRODUCTION**

There is presently much interest in zinc oxide (ZnO) nanostructures due to the variety of possible morphologies that it can form and the ease with which it lends itself to low cost processing. ZnO is an n-type semiconductor material with wide band gap and large exciton binding energy of 3.37 eV and 60 meV respectively. The low variability of the band gap of ZnO with temperature is considered advantageous in applications where temperature stability is important. In addition, ZnO displays a wide variety of structures at the nanoscale such as nanorods, nanowires, nanoflakes and nanoneedles. This opens up a myriad of potential applications in the medical and technological industries, hence its present popularity as an important research material. ZnO has found application in surface acoustic wave (SAW) filters, photonic crystals, light emitting diodes, photo-detectors, optical

modulator waveguides, varistors, gas sensors, dye sensitized solar cells, field emission, photo-catalysts and many others [1, 2]. The particular morphology, size and orientation may further our understanding of quantum effects, electrical and optical properties [3-6]. A better grasp of the conditions of the formation of these nanostructures may also lead to improved, novel nanostructures with improved functionality or altogether new and unique properties. The growing body of the literature reports many and varied synthesis techniques for the different nanostructures of ZnO [7-12]. The authors have themselves previously reported successful synthesis and investigations of ZnO nano-needles using a zinc-air cell system (ZAC) [14, 15]. The XRD studies appear to suggest that this method allows different nanostructures to be obtained depending on the variation of parameters such as discharge time and electrolyte type. Therefore, in this paper, we investigate and outline the feasibility of synthesizing different nanostructures by varying electrolyte concentration at fixed annealing temperature.

## 2. EXPERIMENTAL

Solutions of pure sodium hydroxide of different concentration ranging from 0.5 to 2M were prepared in distilled water using commercial sodium hydroxide pellets CP of 2, 4, 6 and 8g of NaOH respectively from Associated Chemical Enterprises (Pty) Ltd. A homogeneously mixed solution was obtained under constant magnetic stirring at room temperature. The solutions were then cooled to room temperature before being injected into the cell enclosure containing a large area of 99.9% by mass pure zinc and an air cathode composed of steel wool and recycled void paper to allow the transfer of electrons from the anode to the cathode. The cell was then allowed to discharge over one hour into a 470 $\Omega$  resistor. The use of the constant load is to keep the discharge current, which doubles as a deposition current, reasonably constant over the discharge time of the cell. This is plausible since the cell output voltage was more or less steady  $\sim$ 1.1V during the experimental runs. The motivation for this is the widely reported effect of discharge current on the observable nanostructures that are formed. After the discharge the zinc plate was removed and cut into several 1x1cm<sup>2</sup> pieces before annealing at 450°C for 60mins. CuK $\alpha$  radiation of XRD of 1.5418Å wavelength was used to determine the crystal structure. Particle morphology and chemical composition of the samples were studied using the Joel JSM-9800F Field Emission scanning electron microscope (FE-SEM) equipped with a dispersive x-ray spectrometer (EDS). The optical properties were studied using a Perkin-Elmer Lambda 950 UV-Vis spectrometer [14-16].

## 3. RESULTS AND DISCUSSION

### 3.1. Crystal structure versus concentration.

Figure 1 shows the XRD patterns of the synthesized ZnO nanostructures at a uniform annealing temperature of 450°C and varying electrolyte concentration. All the observable diffraction peaks in the figure are assigned to either hexagonal ZnO or pure hexagonal zinc (standard JCPDS cards: 80-0075 and 04-0831 respectively). The X-ray reflection planes are (100), (002), (101), (102), (110), (103),

(200), (112) and (200) and correspond to the  $2\theta$  angles of  $31.8^\circ$ ,  $34.4^\circ$ ,  $36.3^\circ$ ,  $47.5^\circ$ ,  $56.5^\circ$ ,  $62.7^\circ$ ,  $66.3^\circ$ ,  $67.9^\circ$  and  $69.0^\circ$ .

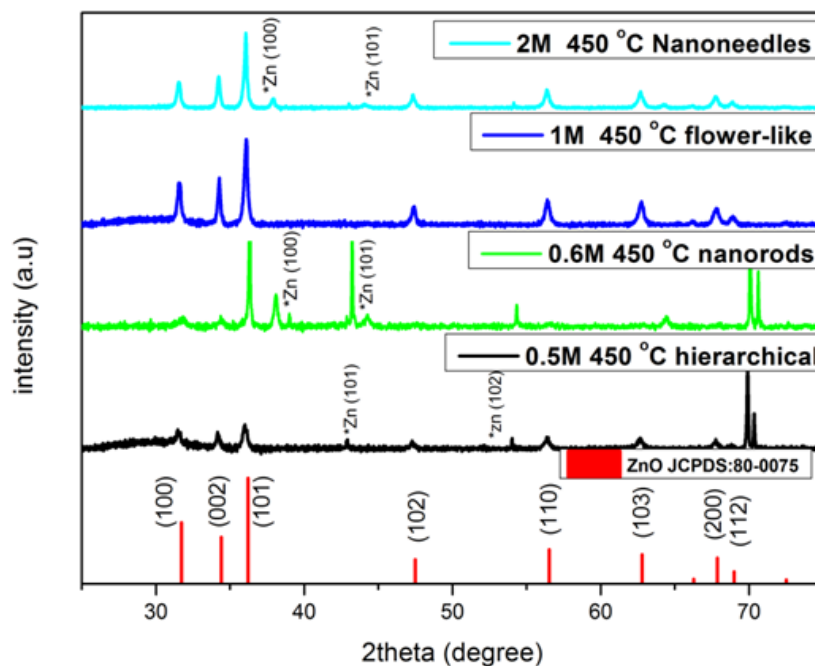


**Figure 1.** XRD patterns of ZnO nanostructures versus concentration at fixed annealing temperature.

The other prominent diffraction peaks in the figure (labeled as \*Zn) conform to pure hexagonal-structured zinc. No foreign impurities were observed. The figure suggests that as the concentration increases the crystallographic structure changes resulting in the formation of hierarchical nanowires, nanorods, flower-like and nano-needle structures which are in agreement with FE-SEM images. Application of the Debye-Scherrer equation [12, 14] with a Scherrer constant of 0.9 gives the results in Table 1.

**Table 1.** Shows the ZnO nanostructures, the  $2\theta$  value, the annealing temperature value and particle sizes

Concentration (M)	ZnO Nanostructure	$2\theta$ (degrees)	Particle sizes (nm)
0.5	Nanowires	36.01	24.49
0.6	Nanorods	36.32	86.18
1	Flower-like	36.08	29.01
2	Nano-needles	36.05	34.52

Table 2 summarizes the lattice parameters  $a$  and  $c$  obtained assuming first order diffraction on the (100) with the angles:  $36.01^\circ$ ,  $36.32^\circ$ ,  $36.08^\circ$  and  $36.05^\circ$ .

**Table 2.** Shows the estimated hexagonal structure lattice constants

ZnO Nanostructure	FWHM (100)	$2\theta$ (degrees)	Lattice $a$ (nm)	Lattice $c$ (nm)
Nanowires	0.3596	31.5090	3.2746	5.6719
Nanorods	0.3091	31.7169	3.2537	5.6356
Flower-like	0.2849	31.5733	3.2681	5.6606
Nano-needles	0.2902	31.5417	3.2713	5.6661

### 3.2. Morphology and chemical analysis

The effect of the NaOH concentration on the final morphology of ZnO nanoparticles was studied by FE-SEM. The results are shown in Figure 2 (a)-(d). The heat treatment temperature used to produce the ZnO morphologies was fixed at  $450^\circ\text{C}$ . Figure 2 (a) shows hierarchical ZnO nanostructures obtained by synthesizing the material with 0.5M concentration. Hierarchical ZnO nanostructures are distributed uniformly and compactly. By controlling the appropriate amount of concentration, the hierarchical structure was transformed into nanorods as shown in Figure 2 (b). Further increase in electrolyte concentration resulted in a flower-like and nano-needles nanostructures as shown Figure 2 (c)-(d). The changes in morphology are thought to arise because of the increase in ionic conductivity as the electrolyte concentration increases. Similar results were observed by Ridhuan et al [18] although their focus was on the transformation of inhomogeneous ZnO nanorods into homogeneous well aligned nano-needles. Moazzen et al have also reported the transformation of ZnO particles from spherical nanoparticles to cauliflower-like nanostructures when the concentration ratio is increased [19]. Liu et al [20] have also investigated the growth of ZnO films having controlled morphology by varying the concentration of NaCl additive in the reactant. They suggest that the resulting variation of ZnO-film morphology is due to the enhanced ionic strength of the electrolyte. This is thought to be due to the promotion of both the concentration of the reactants and also the specific adsorption of organic groups. Similar results were also obtained by Yin et al [21], although their primary focus was on nano-rods obtained over a wide range of concentrations and treatment temperatures. The chemical analysis for ZnO nanostructures using EDS showed no foreign impurities besides carbon which is attributed to post heating as show in Figure 3. However, in spite of the prominent zinc, oxygen and carbon peaks in the EDS spectrum the weight percentage of Zn, and O elements obtained from EDS is nearly stoichiometric.

Figure 2 shows the FE-SEM photographs of the nanostructures summarized in Table 1 and Table 2.

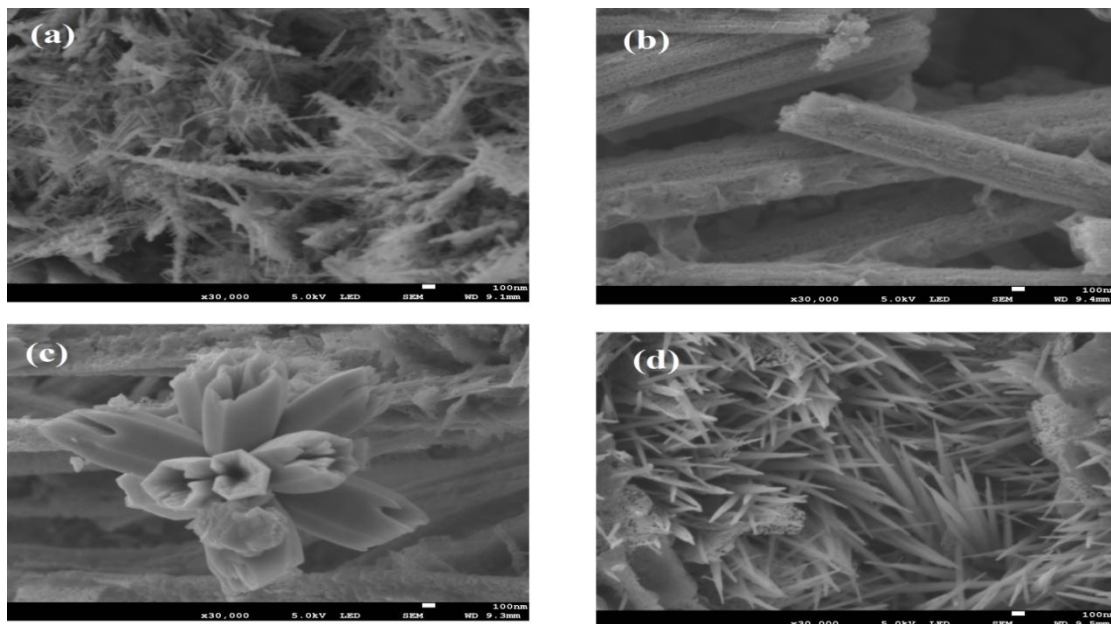


**Figure 2.** FE-SEM images after sample annealing at 450°C versus electrolyte concentration. In (a) hierarchical ZnO nanowires at 0.5M (b) nanorods, 0.6M (c) flower-like at 1.0M and (d) nanoneedles at 2M.

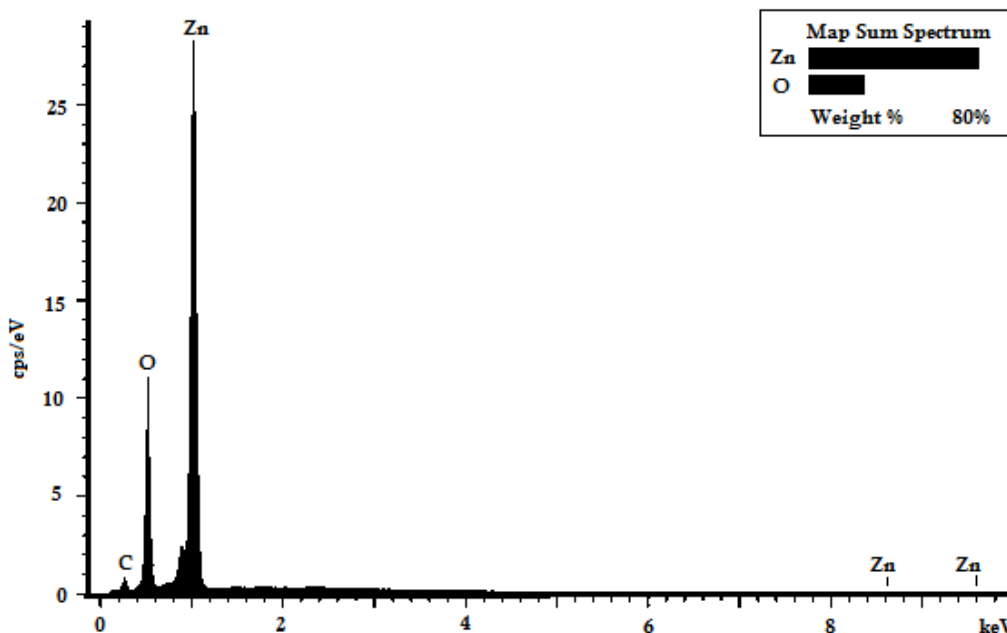


**Figure 3.** Chemical compositions of ZnO nanostructures

### 3.3. Band gap from UV-Vis spectroscopy

Figure 4 shows the UV-Vis spectra of the ZnO nanostructures. The hierarchical nanowires, nanorods, flower-like and nano-needles exhibit two strong absorption peaks between ~300nm-380nm.

The optical absorption of direct band gap ZnO nanostructures can be calculated using the Kubelka–Munk function in Equation (5) and Tauc's relation, Equation (6) [12, 14].

$$F(R) = (1 - R)^2/2R \quad (5)$$

and

$$hv = (F(R) \times hv)^n, \quad (6)$$

where  $R$  is absolute reflectance of the sample layer,  $hv$  is photon energy ( $h$  is Planck's constant and  $\nu$  is photon frequency) and  $n = 0.5$  for a direct band gap semiconductor like ZnO.

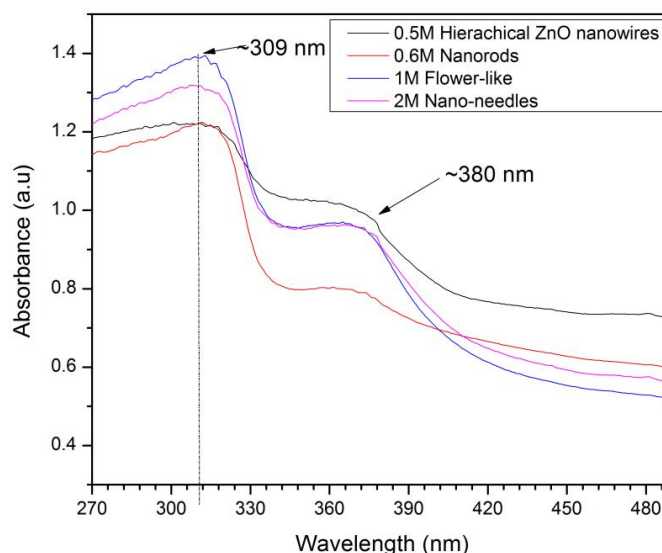


**Figure 4.** UV-Vis absorbance spectra of ZnO nanostructures

The absorption peaks around ~300nm -310nm may be explained in terms of structural defects associated with either Zn or O vacancies. The absorption peaks around ~370nm-380nm conform to the well-known intrinsic band gap absorption of ZnO and indicates that the synthesized nanostructures are in a spatial confinement in contrast to the bulk of ZnO. Figure 5 is the extrapolation of  $(F(R) \times hv)^n$  versus  $hv$ , a technique that leads to the determination of the optical band gap [14]. Table 3 reports the estimated band gaps of the various synthesized nano-structures. The estimated band gaps show low variance between the different nanostructures, averaging 3.1 eV with a variance of ~2.7%. This variance is within the limits of measurement error. It is interesting to note that at the numerically close electrolyte concentrations of 0.5M and 0.6M concentrations two distinct nano-structural forms appear to dominate. There are two possible explanations for this observation. First, there may be a critical concentration at which the one form begins to dominate. Secondly, it is widely reported that the transformation of nanostructures could be due to the non-uniform current distribution on the zinc plates. As the surface profile of the zinc plate changes due to the increasing presence of a given nanostructure, it is likely that there are also localized differences in the current density on plate due to these nanostructures, leading to the formation of different nanostructures around those sites. This possibility is interesting and warrants further investigation.

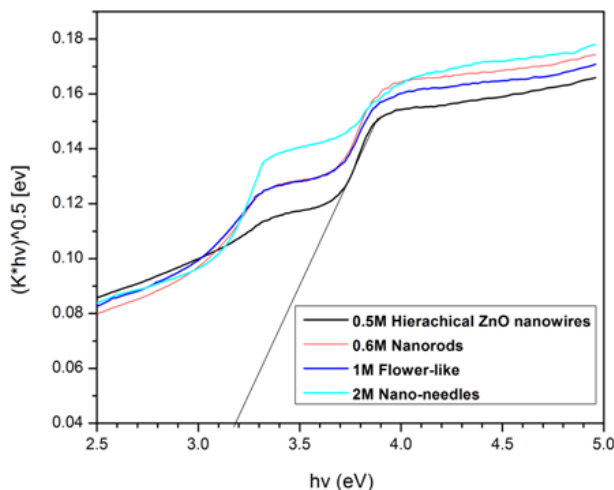


**Figure 5.** Plot of  $(F(R) \times hv)^n$  versus photon energy  $hv$  of ZnO nanostructures

**Table 3.** Estimated optical band gap of ZnO nanostructures

ZnO nanostructure	Band gap (eV)
Nanowires	3.2
Nanorods	3.0
Flower-like	3.1
Nano-needles	3.1

#### 4. CONCLUSIONS

In this paper we extend earlier investigations of the fabrication of ZnO nanostructures using the ZAC system method by suggesting a simple classification of nanostructure as a function of electrolyte concentration. The XRD analysis shows that the synthesized ZnO nanostructures are built on the hexagonal wurtzite structure and that there were no foreign impurities besides the carbon which came as results of post heating. The presence of wire, rod, needle and flower-like nanostructures were confirmed by FE-SEM analysis. The band gaps of these nanostructures were calculated using Tauc’s equation and found to be around 3.1eV for all nanostructures. Therefore, it can be concluded that this method is suitable for the production of ZnO nanostructures that are important in many industrial applications such as LEDs, UV photo detectors, sensing and for other optoelectronic devices.

#### ACKNOWLEDGEMENTS

The authors thank the National Nano-Science Postgraduate Teaching and Training Platform (NNPTTP) and University of the Free State for their financial support.

## References

1. J. Yang, *Sensors*, 13 (2013) 2719-2734
2. X.C. Chen, J.P. Zhou, H.Y. Wang, P.S. Xu and G.P. Pan, *Chines Phys B*, 20 (2011) 096102
3. Y. Tak, K. Yong and C. Park, *J. Cryst. Growth*, 285 (2005) 549–554
4. F. Gu, D. You, Z. Wang, D. Han and G. Guo, *Sens. Actuators, B*, 204 (2014) 342–350
5. V.M. Carrillo-Vázquez and J.G. Murillo, *J. Phys.: Conf. Ser.* 582 (2015) 012053
6. A. Panwar, K.L. Yadav, *Mater Lett* 142 (2015) 30-34
7. Y. Chen, C. Zhang, W. Huang, Y. Situ and H. Huang, *Mater Lett*, 141(2015)294–297
8. M.Ramesh, M. anbuvaran and G. Viruthagiri, *Spectrochim Acta A Mol Biomol Spectrosc.* 2015 Feb 5;136 Pt B:864-70
9. L. Zhang, J. Zhao, H. Lu, L. Li, J. Zheng, H. Li, Z. Zhu *Sens. Actuators B*, 161 (2012) 209–215
10. S. Yilmaz, *J. Supercond Nov Magn*, 27 (2014) 1083-1089.
11. T.T. Miao, D.X. Sun, Y.R. Guo, C. Li, Y. Ma, G.Z. Fang and Q.J. Pan, *Nanoscale Res Lett*, 8 (2013) 431
12. S.K. Chong, C.F. Dee and S.A. Rahman, *Nanoscale Res Lett*, 8 (2013) 1-8
13. T.D. Malevu and R.O. Ocaya, *Int. J. Electrochem. Sci.*, 9 (2014) 8011-8023
14. H. Sun, X. Li, Y. Chen, D. Guo, Y. Xie, W. Li, B. Liu and X. Zhang, *Nanotechnology*, 20 (2009) 425603
15. T.D. Malevu and R.O. Ocaya, *Int. J. Electrochem. Sci.*, 10 (2015) 1752-1761
16. J.P. Mathew, G. Varghese and J. Mathew, *Chin. Phys. B* 21 (2012) 078104
17. H.S. Chin and L.S. Chao, *J Nanomater*, 2013 (2013), Article ID 424953, 8
18. N.S. Ridhuan, K.A. Razak, Z. Lockman, A.A. Aziz, *PLoS One.*, 7(2012) e50405
19. M.A.M. Moazzen, S.M. Borghei, F. Taleshi, *Appl Nanosci.*, 3(2013) 295–302
20. X. Liu, Z. Jin, S. Bu, J. Zhao and Z. Liu, *J. Am. Ceram. Soc.*, 89 (2006) 1226–1231
21. T. Yin, N. Chen, Y. Zhang, X. Cai, Y. Wang, *Superlattices Microstruct.* 74 (2014) 279–293

© 2015 The Authors. Published by ESG ([www.electrochemsci.org](http://www.electrochemsci.org)). This article is an open access article distributed under the terms and conditions of the Creative Commons Attribution license (<http://creativecommons.org/licenses/by/4.0/>).